Clamping Voltage Characteristics and Accelerated Aging Behavior of CoCrTb-doped Zn/Pr-based Varistors with Sintering Temperature

Choon-Woo Nahm*
Semiconductor Ceramics Lab., Department of Electrical Engineering, Dongeui University, Busan 614-714, Republic of Korea

(Received July 27 2009, Accepted August 12 2009)

The clamping voltage characteristics and accelerated aging behavior of CoCrTb-doped Zn/Pr-based varistors were investigated for different sintering temperatures. The best clamping voltage characteristics were obtained for the varistors sintered at 1330°C, with a clamping voltage ratio (K) of 1.63 at a surge current of 5 A and 1.75 at a surge current of 10 A. The varistors sintered at 1330°C exhibited the highest stability, with -0.1% in $\%\Delta E_{1\,mA}$, -0.2% in $\%\Delta\alpha$, and +15.5% in $\%\Delta J_L$ for E-J characteristics under a stress state of 0.90 $E_{1\,mA}$/120°C /24 h. Furthermore, it exhibited $\%\Delta\varepsilon_{APP}'$ of -0.7% and $\%\Delta\tan\delta$ of +5.7% for dielectric characteristics under the same stress state.

Keywords: Sintering, Clamping voltage, DC accelerated aging, Varistors

1. INTRODUCTION

The ZnO varistor is one of the smart electroceramic semiconductor devices, which feature electrical properties deriving from grain boundary effects. ZnO without impurity doping intentionally exhibits nonlinear properties at any sintering condition, whereas ZnO doped with minor metal oxides, such as Pr, Bi, Ba, etc., exhibits remarkably nonlinear electrical properties, which leads to the decrease of impedance with increasing voltage.

The nonlinearity of conduction characteristics is due to the presence of a double electronic potential barrier formed at the active grain boundaries which contain many electronic trap states. Because of their highly nonlinear electrical properties, ZnO varistors are used widely in the field of overvoltage protection systems for electric and electronic systems[1,2]. Commercial ZnO varistors are generally divided into two categories, i.e. Bi-based and Pr-based ceramics. Bi-based ZnO varistors have been studied in different aspects since the discovery of ZnO nonlinear ceramics. Although Bi-based ZnO varistors show good nonlinear properties, Bi_2O_3 easily reacts with some metals used in preparing multilayer chip nonlinear varistors, and it destroys the multilayer structure[3]. In addition, it is reported to have an additional insulating spinel phase. This phase acts as a growth moderator for ZnO grain, but plays no role in the nonlinear electrical characteristics[4]. Furthermore, it also deteriorates the surge-absorption capabilities due to the decrease of effective grain boundary area.

In order to overcome these problems, Pr-based ZnO varistors have been studied by many researchers[5-17]. It is important to comprehend the effect of additives-doping and the sintering process on the application characteristics as well as the basic properties of the varistors[8-17].

In practical varistor applications, two important factors that should be considered are clamping voltage characteristics and accelerated aging characteristics. If the varistor has a high clamping voltage ratio, the varistor cannot absorb a high-energy surge. On the other hand, the varistors begin to degrade because of a leakage current which gradually increases with stress time. Eventually, this results in thermal runaway and the loss of varistor function. Therefore, the electrical stability of the varistor is more important than any other property[10]. The basic varistor characteristics of this paper have been reported previously[18].

The purpose of this paper is to investigate the effect of sintering temperature on the clamping voltage characteristics for specified surge current and the DC accelerated aging behavior of the nonlinear electrical properties and dielectric characteristics for the CoCrTb-doped Zn/Pr-based varistors was investigated and new results were obtained.

2. EXPERIMENTAL PROCEDURES

2.1 Sample preparation

Reagent-grade raw materials were used in the proportions of (97.25) mol% ZnO, 0.5 mol% Pr_6O_{11}, 1.0 mol% CoO, 0.5 mol% Cr_2O_3, and 0.75 mol% Tb_4O_7. Raw materials were mixed by ball milling with zirconia balls and acetone in a polypropylene bottle for 24 h. The mixture was dried at 120°C for 12 h and calcined in air at 750°C for 2 h. The calcined mixture was pulverized using an agate mortar/pestle and after 2 wt% polyvinyl alcohol (PVA) binder addition, granulated by sieving with a 100-mesh screen to produce starting powder. The powder was uniaxially pressed into discs of 10 mm in diameter and 2 mm in thickness at a pressure of 80 MPa. The discs were covered with raw powder in an alumina crucible and sintered at three fixed sintering temperatures (1300°C, 1330°C, and 1350°C) in air for 1 h. The sintered samples were lapped and polished to 1.0 mm thickness. The samples were about 8 mm in diameter and 1.0 mm in thickness. Silver paste was coated on both faces of the samples and ohmic contact electrodes were formed by heating at 600°C for 10 min. The electrodes were 5 mm in diameter.

*Author to whom corresponding should be addressed: electronic mail: cwnahm@deu.ac.kr

2.2 Microstructure examination

Both surfaces of the samples were lapped and ground with SiC paper and polished with 0.3 μm-Al_2O_3 powder to a mirror-like surface. The polished samples were thermally etched at 1100°C for 30 min. The surface of the samples was metallized with a thin coating of Au to reduce charging effects and to improve the resolution of the image. The surface microstructure was examined by a scanning electron microscope (SEM) (Hitachi S2400, Japan). The average grain size (d) was determined by the lineal intercept method, given by d=1.56L/MN, where L is the random line length on the micrograph, M is the magnification of the micrograph, and N is the number of the grain boundaries intercepted by the lines[19]. The sintered density (ρ) of ceramics was measured by the Archimedes method.

2.3 V-I measurement

The electric field-current density (E-J) characteristics of the varistors were measured using a high voltage source measure unit (Keithley 237). The breakdown field ($E_{1\,mA}$) was measured at a current density of 1.0 mA/cm^2 and the leakage current (J_L) was measured at 0.80 $E_{1\,mA}$. In addition, the non-ohmic coefficient (α) is defined by the empirical law, $J = K \cdot E^{\alpha}$, where J is the current density, E is the applied electric field, and K is a constant. α was determined in the current density range of 1.0 mA/cm^2 to 10 mA/cm^2, where $\alpha = 1/(\log E_2 - \log E_1)$, and E_1 and E_2 are the electric fields corresponding to J_1 = 1.0 mA/cm^2, J_2 = 10 mA/cm^2, respectively.

2.4 Clamping voltage measurement

The clamping voltage (V_c) was measured by an impulse surge current wave (8×20 μs) of 5 A and 10 A using a surge generator (Taeyang Eng.) and oscilloscope (TeK 3020B). The clamping voltage ration (K) is defined by ratio of surge voltage to varistor voltage ($V_{5\,A}/V_{1\,mA}$ or $V_{10\,A}/V_{1\,mA}$). The varistor voltage ($V_{1\,mA}$) was measured at a current of 1.0 mA DC.

2.5 DC accelerated aging measurement

The stability against DC accelerated aging stress was performed under the following continuous states;

(i) First stress: 0.85 $E_{1\,mA}$/115°C/24 h,

(ii) Second stress: 0.90 $E_{1\,mA}$/120°C /24 h,

Simultaneously, the leakage current during the stress time was monitored at intervals of 1 min by a high voltage source-measure unit (Keithley 237). The system stressed was applied to the electrical characteristics after storage at normal room temperature for 2 h. The degradation rate coefficient (K_T) was calculated by the expression $I_L = I_{Lo} + K_T t^{1/2}$[20], where I_L is the leakage current at stress time (t) and I_{Lo} is I_L at t = 0. After the respective stresses, the V-I characteristics were measured at room temperature.

Five samples (sintered at the same sintering temperature) were used for all electrical and dielectric measurements and dielectric measurements and the average value was presented.

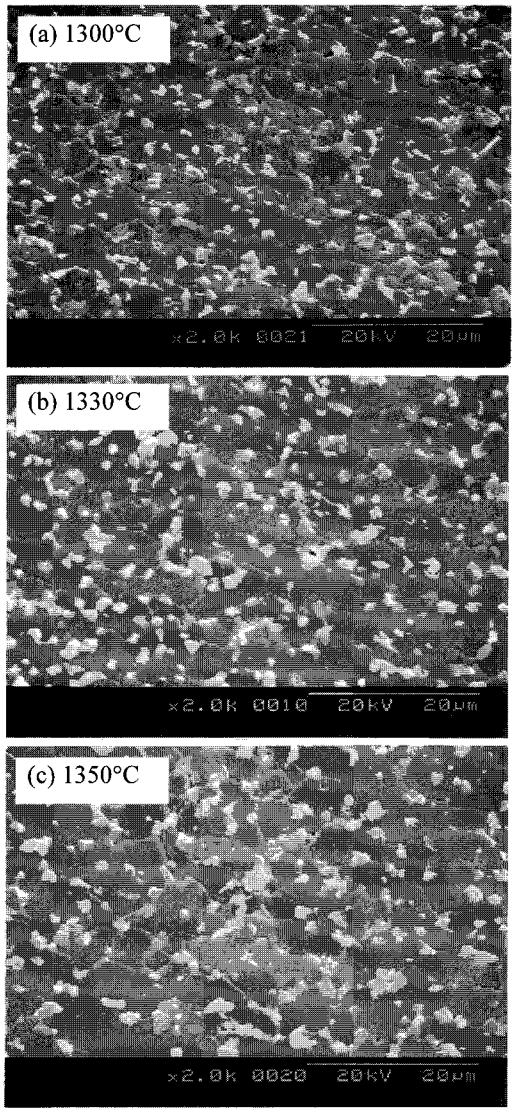

Fig. 1. SEM images of the samples for different sintering temperatures.

3. RESULTS AND DISCUSSION

3.1 Microstructure analysis

Figure 1 shows the SEM images of the samples for different sintering temperatures[18]. The grains were uniformly distributed through the entire samples bulk. The average grain size increased linearly with temperature over the range of samples from 4.3 to 5.1 μm and became constant at sintering temperatures beyond 1330°C. The microstructure consisted of a primary phase of ZnO grains (almost black in color), and intergranular layer as a secondary phase (almost whit in color), which are Pr- rich and Tb-rich phases. Added Pr_6O_{11} and Tb_4O_7 were segregated to grain boundaries and nodal points, Pr-oxide and Tb-oxide were found to coexist in the grain boundaries and the nodal points as if they were a single phase. The overall sample density increased negligibly in the range of 5.81 to 5.82 g/cm^3. This is a very high density so that there was no porosity through the surface microstructure. The high density obtained by sintering is very important for the production of the varistors with high energy capability.

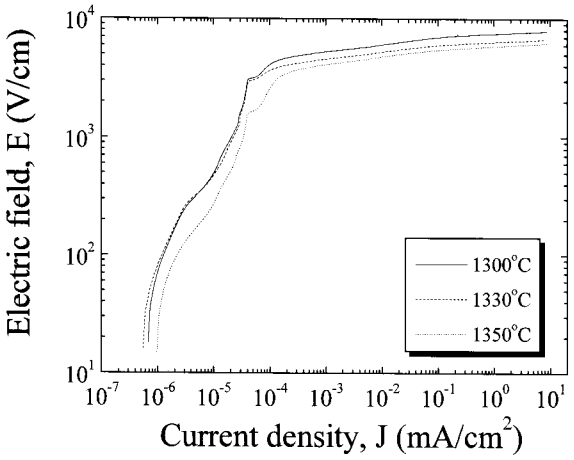

Fig. 2. E-J characteristics of the samples for different sintering temperatures.

3.2 E-J characteristics

Figure 2 shows the E-J characteristics of the samples for different sintering temperatures[18]. The breakdown field ($E_{1\,mA}$) decreased in the range of 7,531 to 5,882 V/cm with increasing sintering temperature. All of the samples provide a very high varistor voltage per unit thickness. This is very important for high voltage nonlinear ceramics with a compact size. The decrease of $E_{1\,mA}$ with increasing sintering temperature can be explained by the grain size based on the inverse relationship between varistor voltage and average grain size.

The nonlinear coefficient (α) decreased in the range of 46 to 36 with increasing sintering temperature. The sintering temperature has a significant effect on nonlinear properties. Many ions migrate to the interior and exterior of the grains when the sintering temperature increases. As a result, the electronic states will vary at grain boundaries and lead to any variation in the potential barrier. The leakage current density (J_L) was in the range 7.24 to 9.49 $\mu A/cm^2$. The detailed electrical parameters are summarized in Table 1.

3.3 Surge clamping characteristics

Figure 3 shows the clamping voltage (V_c) characteristics for different sintering temperature. The V_c is defined by the drop voltage between electrodes of sample when the specified surge current (5 A for electrode diameter ϕ5 mm or 10 A for disc diameter ϕ7 mm) flows through sample. The surge current is specified in IEC with a sample size[23]. The higher surge current leads to the higher V_c. All the

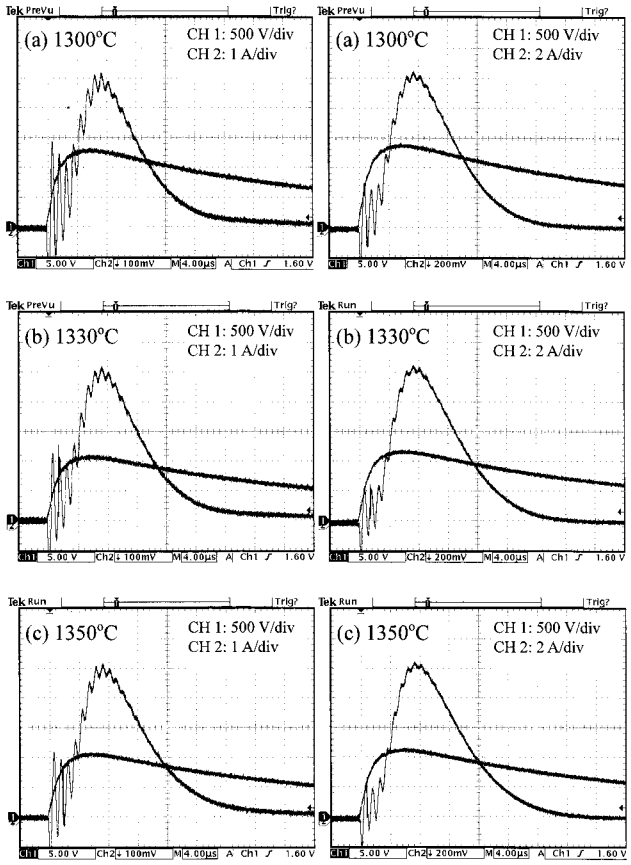

Fig. 3. Clamping voltage characteristics for different sintering temperatures.

samples clamped to the specified voltage for a surge current of 5 A (Fig. 3(a)) and 10 A (Fig. 3(b)). The detailed clamping voltage against surge current is summarized in Table 1. The samples sintered at 1300°C, 1330°C, and 1350°C exhibited a clamping voltage ratio (K) of 1.68, 1.63, and 1.74 at a surge current of 5 A, respectively. In addition, the K values at a surge current of 10 A exhibited 1.77, 1.75, and 1.85 for respective sintering temperature. As a result, the samples sintered at 1330°C exhibited the best clamping characteristics.

3.4 DC accelerated aging characteristics

Figure 4 shows the variation of leakage current during a few DC accelerated aging stresses of the samples for different sintering temperatures. All the samples exhibited almost constant leakage current for specified stress condition. Higher stress strength caused the leakage current to increase. The stability of the nonlinear properties of the samples can

Table 1. E-J characteristic parameters, clamping voltage (V_C), and clamping voltage ratio (K) of the samples for different sintering temperatures.

Sintering temp. (°C)	$E_{1\,mA/cm^2}$ (V/cm)	α	J_L ($\mu A/cm^2$)	V_{1mA} (V)	V_C (V)		K	
					I_P=5 A	I_P=10 A	I_P=5 A	I_P=10 A
1300	7,531	46	9.5	779	1,310	1,380	1.68	1.77
1330	6,411	44	7.2	664	1,080	1,160	1.63	1.75
1350	5,882	36	8.4	615	1,070	1,140	1.74	1.85

be estimated by the degradation rate coefficient (K_T), indicating the degree of aging from the slope of the I_L-$t^{1/2}$ curve. In general, the lower K_T leads to higher stability. Macroscopically, the sintered density and the leakage current have a significant effect on the stability against stress. That is, the higher the sintered density and the lower the leakage current, the higher the stability. The low sintered density decreases the number of parallel conduction paths and eventually leads to the concentration of current. The high leakage current gradually increases the carrier generation due to Joule heating and it leads to a repetition cycle between Joule heating and leakage current. This is key reason for the aging mechanism from a macroscopic viewpoint. The sintered density for all samples is not low enough to have an effect on the stability, whereas the leakage current exhibited large differences between the samples. All the samples exhibited a relatively high stability, with the negative creep of leakage current (NCLC) under the first stress (0.85 $E_{1\,mA}$/115°C/24 h) and the second stress (0.90 $E_{1\,mA}$/120°C/24 h).

The E-J characteristics for the stressed samples are shown in Fig. 5. On the whole, the pre-breakdown region was mainly affected by the stress, whereas the breakdown region was not very much affected by stress. In particular, the sample sintered at 1330°C exhibited a small variation through the entire E-J characteristic curves compared with other samples. This means that this sample exhibits the highest stability in conduction against DC accelerated aging stress. The variation of the pre-breakdown region with stress is related to the double Schottky barrier at the grain boundaries. The increase of leakage current in the pre breakdown region after stress is attributed to the lowering of the Schottky barrier due to the variation of the electronic state at the grain boundary. The detailed E-J characteristic parameters such as the variation rates of breakdown field ($\%\Delta E_{1\,mA}$), nonlinear coefficient ($\%\Delta\alpha$), and leakage current density ($\%\Delta J_L$) after DC accelerated aging stress are summarized in Table 2. After stress, the $E_{1\,mA}$ varied to within 0.3%, the α varied to within 1.5%, and the J_L varied greatly unlike $E_{1\,mA}$ and α. Of all the samples, the sample sintered at 1330°C exhibited the smallest variation. The $\%\Delta E_{1\,mA}$ was 0.1%, the $\%\Delta\alpha$ was -0.2%, and the $\%\Delta J_L$ was less than +20% under the second stress (0.90 $E_{1\,mA}$/120°C/24 h).

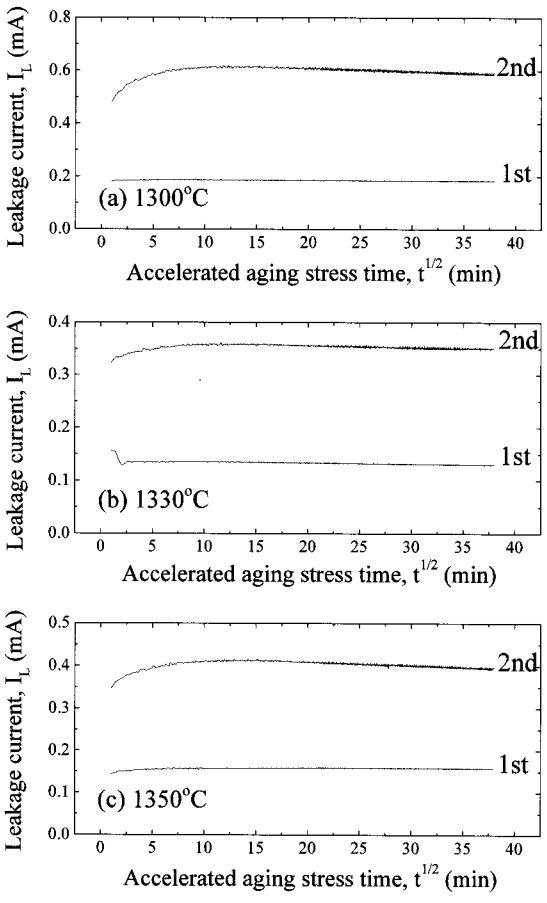

Fig. 4. Leakage current during DC accelerated aging stress for different sintering temperatures.

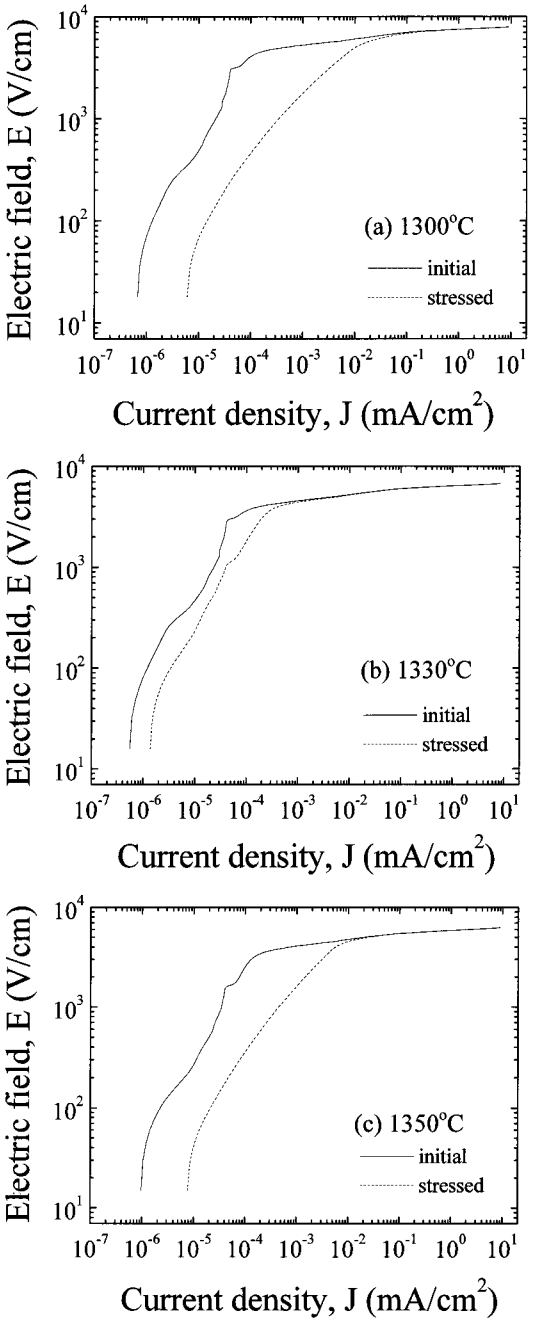

Fig. 5. E-J characteristics before and after DC accelerated aging stress of the samples for different sintering temperatures.

Figure 6 shows the dielectric constant characteristics before and after stress. There are no the variation in these characteristics before and after stress. Therefore, all the samples exhibited very stable dielectric constant characteristics. The detailed dielectric constant before and after stress is shown in Table 3. The variation of dielectric constant after stress for all the samples was less than 1%.

Figure 7 shows the dissipation factor (tanδ) characteristics before and after stress. These curves exhibited large differences between the samples sintered at different temperatures unlike the dielectric constant after stress. In particular, tanδ varied remarkably in the frequency regime less than 1 kHz and it varied very little at frequency exceeding 20 kHz. Of all the samples, the sample sintered at 1330°C exhibited the smallest variation, which the %Δ tanδ is only 6% after the second stress (0.90 $E_{1\,mA}$/120°C/24 h) compared with other samples, as exhibited in Table 2. The tendency of the behavior of %Δ tanδ with respect to sintering temperature after the second stress (0.90 $E_{1\,mA}$/120 °C/24 h) coincided with that of $\%\Delta J_L$.

Concerning stability, the model for instability/stability of varistor ceramics, according to various stresses, is known to be an ion migration mechanism proposed by Gupta and Carlson[21]. The main cause of degradation under external stress is the deformation of the Schottky barriers between the ZnO grains[22]. The donor-like within depletion region consists of greatly stable ionic components and meta-stable ionic components. The factors relating to degradation are meta-stable ions such as zinc interstitial ions: singly positively charged $Zn_i^{\cdot}$ and doubly positively charged $Zn_i^{\cdot\cdot}$.

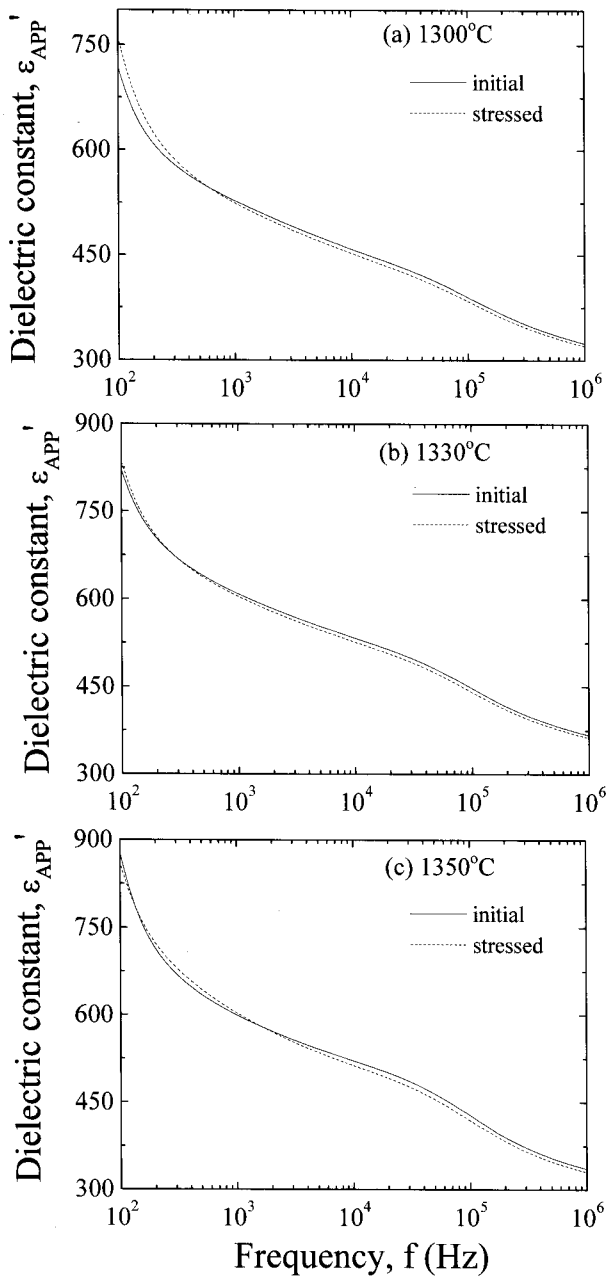

Fig. 6. Dielectric constant characteristics before and after DC accelerated aging stress of the samples for different sintering temperatures.

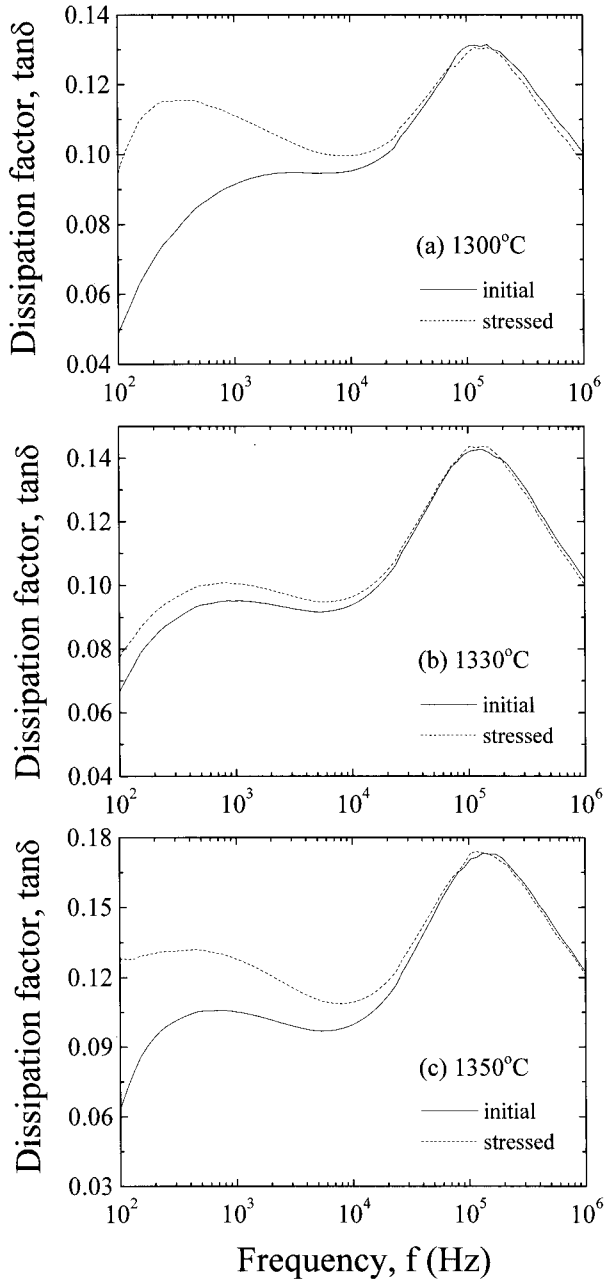

Fig. 7. Dielectric dissipation factor characteristics before and after DC accelerated aging stress of the samples for different sintering temperatures.

Table 2. E-J characteristic parameters before and after DC accelerated aging stress of the samples for different sintering temperatures.

Sintering temp. (°C)	Stress state	K_T ($\mu A \cdot h^{-1/2}$)	$E_{1\,mA}$ (V/cm)	$\%\Delta E_{1\,mA}$	α	$\%\Delta\alpha$	J_L ($\mu A/cm^2$)	$\%\Delta J_L$
1300	Initial	-	7,531	0	45.7	0	9.7	0
	1st	-0.7	7,526	-0.1	45.0	-1.5	15.3	57.9
	2nd	-4.1	7,516	-0.2	44.5	-2.6	26.5	173.7
1330	Initial	-	6,411	0	43.5	0	7.1	0
	1st	-1.5	6,412	0.1	43.5	0	7.7	8.5
	2nd	-2.6	6,410	-0.1	43.4	-0.2	8.2	15.5
1350	Initial	-	5,882	0	35.9	0	8.7	0
	1st	-0.1	5,893	0.2	36.0	0.3	11.2	28.7
	2nd	-5.8	5,899	0.3	36.4	1.4	13.3	52.9

Table 3. Dielectrics characteristic parameters before and after DC accelerated aging stress of the samples for different sintering temperatures.

Sintering temp. (°C)	Stress state	ε_{APP}'	$\%\Delta\varepsilon_{APP}'$	$\tan\delta$	$\%\Delta\tan\delta$
1300	Initial	529.1	0	0.091	0
	1st	514.1	-2.8	0.103	12.6
	2nd	526.2	-0.6	0.111	22.3
1330	Initial	610.3	0	0.095	0
	1st	601.8	-1.4	0.101	6.2
	2nd	606.0	-0.7	0.101	5.7
1350	Initial	601.2	0	0.105	0
	1st	605.0	0.6	0.125	19.0
	2nd	605.3	0.7	0.128	21.8

These ions are relatively mobile compared with other ions. The Zn_i ions diffuse toward grain boundaries under external stress and react with negatively charged Zn vacancies: V_{Zn}' and V_{Zn}''. As a result, this process leads to a reduction of a potential barrier and an increase of leakage current. Therefore, the way to improve the stability is to restrict the generation of Zn_i within the depletion layer or the migration of Zn_i toward grain boundaries. It is proposed that the sintering temperature is closely related to a zinc interstitial (Zn_i) density based on the defect model. Conclusively, the appropriate sintering temperature leads to improvement of stability against stress. However, higher sintering temperature may cause a higher Zn_i density, which degrades the stability.

4. CONCLUSIONS

The clamping voltage characteristics for surge current and DC accelerated aging behavior of E-J and dielectric characteristics of the CoCrTb-doped Zn/Pr-based varistors were investigated at different sintering temperatures. The samples sintered at 1330°C exhibited the best clamping characteristics compared with other samples, with a clamping voltage ratio (K) of 1.63 at a surge current of 5 A and 1.75 at a surge current of 10 A. The highest stability of E-J and dielectric characteristics was obtained for the varistor sintered at 1330°C exhibited, which the $\%\Delta E_{1\,mA}$ was -0.1%, the $\%\Delta\alpha$ was -0.2%, $\%\Delta J_L$ was +15.5% for E-J characteristics, and the $\%\Delta\varepsilon_{APP}'$ was -0.7% and $\%\Delta\tan\delta$ of +5.7% for dielectric characteristics, under stress state of 0.90 $E_{1\,mA}$/120°C /24 h. It can improve the clamping voltage characteristics for surge current and the stability against accelerated aging stress by sintering the samples at the moderate temperature.

REFERENCES

[1] L. M. Levinson and H. R. Philipp, Amer. Ceram. Soc. Bull. **65**, 639 (1986).
[2] T. K. Gupta, J. Amer. Ceram. Soc. **73**, 1817 (1990).
[3] Y. S. Lee and T. Y. Tseng, J. Amer. Ceram. Soc. **75**, 1636 (1992).
[4] J. Wong, J. Appl. Phys. **46**, 1653 (1975).
[5] A. B. Alles and V. L. Burdick, J. Appl. Phys. **70**, 6883 (1991).
[6] A. B. Alles, R. Puskas, G. Callahan, and V. L. Burdick, J. Am. Ceram. Soc. **76**, 2098 (1993).
[7] Y.- S. Lee, K.-S. Liao, and T.- Y. Tseng, J. Amer. Ceram. Soc. **79**, 2379 (1996).
[8] C.-W. Nahm, Mater. Lett. **47**, 182 (2001).
[9] C.-W. Nahm and J.-S. Ryu, Mater. Lett. **53**, 110 (2002).
[10] C.-W. Nahm, Solid State Commun. **126**, 281 (2003)
[11] C.-W. Nahm, Mater. Lett. **57**, 1317 (2003).
[12] C.-W. Nahm and B.-C. Shin, Mater. Lett. **57**, 1322 (2003).
[13] C.-W. Nahm, Mater. Lett. **58**, 2252 (2004).
[14] C.-W. Nahm and B.-C. Shin, J. Mater. Sci.: Mater. Electron. **16**, 725 (2005).
[15] C.-W. Nahm, Mater. Lett. **60**, 3394 (2006).
[16] C.-W. Nahm, Trans. Electr. Electron. Mater. **8**, 105 (2007).
[17] C.-W. Nahm, Mater. Lett. **62**, 2900 (2008).
[18] C.-W. Nahm, Trans. Electr. Electron. Mater. **10**, 80 (2009).
[19] J. C. Wurst and J. A. Nelson, J. Amer. Ceram. Soc. **55**, 109 (1972).
[20] J. Fan and R. Freer, J. Am. Ceram. Soc. 77, 2663 (1994).
[21] T. K. Gupta and W. G. Carlson, J. Mater. Sci. **20**, 3487 (1985).
[22] K. Eda, A. Iga, and M. Matsuoka, J. Appl. Phys. **51**, 2678 (1980).
[23] International Electrothechnical Committee, "IEC 61000-4-series, Electromagnetic Compatibility", IEC publisher, 1992.